

RESEARCH

Open Access



Icariside II induces ferroptosis through the down-regulation of SLC7A11 in ovarian cancer

Donglan Yuan^{1†}, Ting Guo^{2†}, Xiaotong Zhu¹, Weiwei Song³, Dengyun Nie⁴ and Hong Yu^{5,6*}

Abstract

Background Ovarian cancer (OV) is the leading cause of death among gynecological malignancies. This study aimed to investigate the influence of Icariside II on OV *in vitro* and *in vivo* and to elucidate whether Icariside II induces ferroptosis in OV cells by regulating SLC7A11 expression.

Methods SKOV3 cells and OV nude mice were treated with Icariside II, a control-plasmid or an SLC7A11-plasmid. EdU assay, flow cytometry, wound-healing assay, and Transwell assays were used to assess cell proliferation, apoptosis, migration, and invasion respectively. Total iron, Fe²⁺ levels, and intracellular lipid reactive oxygen species (ROS) stimulation were evaluated in both cells and tissues. Levels of cysteine (Cys), glutathione (GSH), and glutathione peroxidase 4 (GPX4) were also analyzed. Ferroptosis markers, including Ptg2, Chac1, SLC7A11, and apoptosis-associated genes (Bax and Bcl-2), were detected using qRT-PCR, western blotting, and immunohistochemistry (IHC). SLC7A11 expression in OV was explored using data from The Cancer Genome Atlas (TCGA), and validated with IHC staining.

Results Icariside II-induced ferroptosis in OV cells was confirmed by elevated Fe²⁺ and total iron levels, enhanced lipid ROS levels, higher Ptg2 and Chac1 mRNA levels, and reduced levels of SLC7A11, Cys, GSH, and GPX4 in both *in vitro* and *in vivo* models. These effects were partially reversed by the SLC7A11-plasmid. Moreover, Icariside II suppressed SKOV3 cell proliferation, inhibited cells migration and invasion, and promoted apoptosis by downregulating SLC7A11 expression. Furthermore, we found that SLC7A11 expression was upregulated in OV tissues compared to adjacent non-tumor tissues.

Conclusion Icariside II induces ferroptosis in OV by downregulating SLC7A11 expression *in vitro* and *in vivo*. Our study identified Icariside II as a promising therapeutic agent for the treatment of OV.

Keywords Icariside II, Ferroptosis, SLC7A11, Ovarian cancer

[†]Donglan Yuan and Ting Guo contributed equally to this work.

*Correspondence:

Hong Yu

yuhong@njmu.edu.cn

¹Department of Obstetrics and Gynecology, Affiliated Taizhou People's Hospital of Nanjing University of Traditional Chinese Medicine, Taizhou 225300, China

²Center for Molecular Medicine, Affiliated Taizhou People's Hospital of Nanjing University of Traditional Chinese Medicine, Taizhou 225300, China

³Department of Traditional Chinese Medicine, Affiliated Taizhou People's Hospital of Nanjing University of Traditional Chinese Medicine, Taizhou 225300, China

⁴Nanjing University of Traditional Chinese Medicine, Nanjing 210023, China

⁵Department of Pathology, Affiliated Taizhou People's Hospital of Nanjing University of Traditional Chinese Medicine, Taizhou 225300, China

⁶Affiliated Taizhou People's Hospital of Nanjing University of Traditional Chinese Medicine, No. 399 Hailing Road, Taizhou 225300, China



Introduction

Ovarian cancer (OV) is one of the most common female cancers among gynecological malignancies in the world [1]. In 2022, the newly issued case of ovarian cancer was 324,398, accounting for 1.6% of the total cancer cases; the death case was 206,839, accounting for 2.1% of the total cancer cases [2]. The etiology of OV remains unclear, but its onset may be associated with factors including age, fertility, blood type, psychological factors, and environment [3, 4]. Owing to the high heterogeneity of OV and lack of reliable detection markers, most patients are diagnosed at an advanced stage. Immunotherapy, hormone therapy, and targeted therapy are the primary treatments for ovarian cancer [5–7]. Despite the high initial response rate to chemotherapy, many patients develop recurrent disease accompanied by chemotherapy resistance, ultimately leading to a low 5-year survival rate. Therefore, it is crucial to further explore the mechanism underlying OV and identify new therapeutic targets to improve treatment outcomes.

Ferroptosis is a newly discovered cell death pattern that relies on intracellular free iron (Fe^{2+}) and differs from other forms of cell death such as apoptosis, necrosis, and autophagy, in morphology, biochemistry, and genetics [8, 9]. Abnormal increases in intracellular iron levels can cause an imbalance in cell membrane redox and lipid peroxidation, eventually leading to cell death [10]. In recent years, numerous studies have linked ferroptosis to various diseases, including cancer, ischemic organ damage, and cardiovascular disease [11, 12]. Qi et al. observed that the lncRNAs GABPB1-AS1 and GABPB1 regulate oxidative stress during erastin-induced ferroptosis in HepG2 hepatocellular carcinoma cells [13]. He et al. found that tanshinone IIA protects human coronary artery endothelial cells from ferroptosis by activating the NRF2 pathway [14]. However, the specific mechanisms underlying ferroptosis in OV require further exploration.

Herba Epimedii, a Chinese herbal medicine with a long history, is known for its effects in tonifying kidney yang, strengthening muscles and bones, and dispelling wind and dampness [15]. Icaritin, one of the main active ingredients in Herba Epimedii, plays an important role in preventing congestive heart failure and hypertension, regulating the immune system, and protecting the cardiovascular system [16]. Icariside II, the main metabolite of icaritin, has various pharmacological activities, including liver protection, anti-osteoporosis, anti-inflammatory, and antioxidant activities [17]. Yuan et al. found that Icariside II suppresses tumorigenesis and the progression of ovarian cancer by regulating the miR-144-3p/IGF2R axis [18]. Yu et al. found that Icariside II induces ferroptosis in renal cell carcinoma cells by regulating the miR-324-3p/GPX4 axis [19]. However, the role of Icariside II in inducing ferroptosis in OV remains unclear.

Thus, our study was designed to (i) explore whether Icariside II can induce ferroptosis in OV cells, (ii) investigate whether Icariside II can regulate the expression of SLC7A11 in OV, and (iii) analyze the regulatory mechanism by which Icariside II induces ferroptosis in OV through the regulation of SLC7A11 expression, to identify a promising target for OV therapy.

Materials and methods

Cell culture

SKOV3 cells were obtained from ATCC and cultured in DMEM (Gibco; USA) supplemented with 15% FBS and 1% penicillin/streptomycin (Gibco; USA) in a humidified incubator with 5% CO_2 at 37 °C. SKOV3 cells were treated with 0, 20, 40, or 60 μM Icariside II for 48 h for subsequent experiments.

Iron assay

The total iron (E-BC-K880-M, Elabscience) and Fe^{2+} (E-BC-K881-M, Elabscience) levels in SKOV3 cells were measured per as the manufacturer's instructions. Briefly, 1×10^6 cells were collected and added with 0.2 ml reagent 1, then the cells were placed on ice for lysis for 10 min. Subsequently, the cells were centrifuged at 15,000 $\times g$ for 10 min, and the supernatant were collected for later use. For total iron detection, 80 μl supernatant were added with 80 μl reagent 2 and then incubated at 37 °C for 40 min. For Fe^{2+} detection, 80 μl supernatant were added with 80 μl reagent 3 and then incubated for 40 min at 37 °C. Finally, absorbance at 593 nm was measured to determine the total iron and intracellular Fe^{2+} concentration using a microplate reader (SMR16.1, USCNK).

The total iron (E-BC-K772-M, Elabscience) and Fe^{2+} (E-BC-K773-M, Elabscience) levels in tumor tissues were detected following with the manufacturer's instructions.

Lipid reactive oxygen species (ROS) assay

ROS fluorescent method test kit (E-BC-K138-F, Elabscience) was used to detect the ROS levels according to the protocol. After treatment, SKOV3 cells were collected by centrifugation at 4 °C for 5 min. The cells were then incubated with DCFH-DA staining solution and cultivated for 30 min at 37 °C. Finally, fluorescence was examined using a FACS Aria II flow cytometer (BD Technologies). The ROS levels in tumor tissues were determined using the microplate reader (SMR16.1, USCNK) according to the manufacturer's instructions.

qRT-PCR analysis

After treatment, the levels of Ptgs2, Chac1, SLC7A11, Bax, and Bcl-2 were measured using qRT-PCR. RNA was isolated from SKOV3 cells or tissues using TRIpure Total RNA Extraction Reagent (EP013, ELK Biotechnology), following the manufacturer's protocol. Total RNA

was then reverse transcribed into cDNA using the cDNA Synthesis Kit (Eq. 031, ELK Biotechnology), and qRT-PCR analysis was conducted using SYBR Green Master mix (Eq. 001, ELK Biotechnology) with an ABI 7500 Real-Time PCR System (Life Technologies). Target gene expressions were quantified using the $2^{-\Delta\Delta C_t}$ method. Primer sequences for PCR were listed in Table 1.

Western blot assay

After treatment, proteins were extracted from SKOV3 cells using radioimmunoprecipitation assay (RIPA) buffer (AS1004, ASPEN) for 30 min on ice. Proteins were separated using SDS-PAGE (AS1012, ASPEN) and transferred onto polyvinylidene fluoride (PVDF) membranes. The membranes were blocked with 5% skimmed milk for 2 h to avoid nonspecific binding and then incubated with primary antibodies against SLC7A11 (ab175186, 1:3000, Abcam), Bax (#2772, 1:2000, CST), Bcl-2 (ab196495, 1:3000, Abcam), or β -actin (EA014, 1:10000, ELK Biotechnology) at 4 °C overnight. After washing the membrane thrice with TBST, the membranes were incubated with secondary antibodies for 2 h. Protein signals were assessed using the ECL method (AS1059, ASPEN) according to the manufacturer's instructions.

Cystine (Cys), glutathione (GSH) and glutathione peroxidase 4 (GPX4) level measurements

After treatment, the SKOV3 cells were gently washed with pre-cooled PBS, trypsinized, and centrifuged at 1000×g for 5 min. The cells were then washed three times with pre-cooled PBS, and resuspended in fresh lysis buffer. The levels of Cys, GSH, and GPX4 were measured using the Human Cysteine ELISA Kit (ELK9092, ELK

Biotechnology), Glutathione assay kit (A006-2, Nanjing Jiancheng Bioengineering Institute), and Human GPX4 ELISA Kit (ELK4775, ELK Biotechnology), respectively, following the manufacturer's instructions.

Cell transfection

After treatment, the SKOV3 cells were transfected with control-plasmid or SLC7A11-plasmid using Lipofectamine® 3000 reagent (Thermo) for 24 h following the instructions. qRT-PCR and western blotting were then performed to evaluate cell transfection efficiency.

EdU assay

After treatment, the EdU assay was performed on SKOV3 cells using EDU cell proliferation test kit (C10310-3) according to the manufacturer's instructions. Briefly, SKOV3 cells were plated into 96-well plates and cultured for 2 h after treatment with 50 μ M EdU. The cells were fixed with 4% paraformaldehyde and stained using the Apollo reaction kit. Results were quantified by counting five random fields using a CytoFLEX flow cytometer (Beckman Coulter, USA).

Flow cytometry analysis

After treatment, SKOV3 cells were plated into 96-well plates and cultured for 24 h at 37 °C. The cells were collected by centrifugation at 4 °C for 5 min and then washed with PBS. Cell apoptosis was detected using the Annexin V-FITC/PI Apoptosis Detection Kit (556547, BD Biosciences) following the manufacturer's instructions. Apoptosis was assessed using a BD Aria III flow cytometer (BD Technologies).

Wound-healing assay

After treatment, the SKOV3 cells were seeded in 96-well plates. Lines were drawn evenly behind the 96-well plate using a marker. When the cells reached approximately 90% confluence, the pipette tip was placed perpendicular to the drawn line to create a linear scratch. The cells were washed with PBS three times, and the scratched cells were removed, and serum-free medium was then added. Cells were cultured in a 5% CO₂ incubator at 37 °C, and photographed at 0 and 24 h. The size of the wound gap was then measured.

Transwell assay

After treatment, SKOV3 cells were incubated in a serum-free medium for starvation and seeded into the upper chamber of the Transwell chambers with Matrigel (BD Biosciences). After culturing for 48 h, the remaining SKOV3 cells in the upper chamber (non-migrated) or on the ECM gel-coated surface were removed using a cotton swab. Cells adhering to the lower surface of the membrane were fixed with 4% paraformaldehyde and stained

Table 1 Primer sequences for PCR

Gene	Sequences(5'-3')
H-ACTIN	sense GTCCACCGCAAATGCTTCTA
	antisense TGCTGTACCTTACCAGGTTTC
H-Ptgs2	sense AGATTATGTGCAACACTTGAGTGG
	antisense ATTCCTACCACCAGCAACCCT
H-Chac1	sense GTGGTGACGCTCCTTGAAGAT
	antisense GCCTCTCGCACATTCAGGTAC
H-SLC7A11	sense TGTGGGGTCCCTGCTACTATTG
	antisense GATATCACAGCAGTAGCTGCAGG
H-Bax	sense TCTGAGCAGATCATGAAGACAGG
	antisense ATCCTCTGCAGCTCCATGTTAC
H-Bcl-2	sense AGGATTGTGGCCTTCTTGTAG
	antisense AGCCAGGAGAAATCAAACAGAG
M-SLC7A11	sense AAGGGCATACTCCAGAACACG
	antisense GCCAGCAAAGGACCAAAGAC
M-Ptgs2	sense AGGGAATAAGGAGCTTCTCTG
	antisense CCAATGACCTGATATTTCAATTT
M-Chac1	sense AGCCGGACTTTGCTATATGTG
	antisense TCCTCACATTCAGGTACTTCAG

with 0.1% crystal violet for 10 min. Cells were observed and counted in five random fields under a microscope (Nikon, Tokyo, Japan).

Animal studies

Nude mice were purchased from the SLAC Laboratory Animal Co., Ltd. (Shanghai, China). All mice were housed in a specific pathogen-free environment with a standard light-dark cycle at 25 °C for 12 h and had free access to food and water. SKOV3 cells were then injected subcutaneously into nude mice with 100 μ L normal saline. Tumor volume (V) was calculated using the formula: $V = L \times W^2/2$, where L is the tumor length and W is the tumor width. Tumors were collected and weighed from all mice after humane euthanasia. Animal care and experimental procedures were approved by the Animal Ethics Committee of Jiangsu Hanjiang Biotechnology Co., Ltd. (approval number: HJYB-23092001).

IHC analysis

OV tissues and adjacent normal tissues were fixed with 4% paraformaldehyde for 24 h, embedded in paraffin, and sectioned. The slices were incubated in the citric acid buffer for 10 min and baked in an oven at 62 °C for 90 to 120 min. The slides were then sealed with 5% BSA for 30 min and then incubated overnight at 4 °C using SLC7A11 (1:200, Triple Eagle, 26864-1-AP). These sections were subsequently incubated with a secondary antibody for 30 min, stained with hematoxylin for 3 to 10 min, and observed under an optical microscope (OLYMPUS).

Clinical samples

Cancer and adjacent normal tissues from patients with OV were collected aseptically at the Affiliated Taizhou People's Hospital of Nanjing University of Traditional Chinese Medicine. The tissues were rapidly frozen and stored in liquid nitrogen. Written informed consent was obtained from each patient before participation. This study was approved by the Ethics Committee of the Affiliated Taizhou People's Hospital of the Nanjing University of Traditional Chinese Medicine (Approval number KY-2024-174-01).

Data source

Data of OV patients including expression of SLC7A11 and matching clinical information (such as pathologic stage, histologic grade, overall survival (OS), and sex) were obtained from The Cancer Genome Atlas (TCGA) database. Pan-cancer and OV-related gene expression data were also retrieved from the TCGA database (<https://genomecancer.ucsc.edu/>).

Statistical analysis

Statistical analyses were conducted using GraphPad Prism software (version 6.0). All findings are displayed by mean \pm standard deviation (SD) from three independent experiments. Mean differences among groups were estimated using the unpaired Student's t-test or one-way ANOVA. * $P < 0.05$, and ** $P < 0.01$ indicated as significant difference.

Results

Icariside II-induced ferroptosis in OV cells by regulating SLC7A11 expression

Ferroptosis is an iron-dependent form of cell death distinct from apoptosis, necrosis, and autophagy. An increasing number of studies have shown that the process of ferroptosis involves divalent iron or ester oxygenase, as well as the antioxidant system of oxygenase and the cystine/glutamate reverse transporter [20]. To investigate whether Icariside II induces ferroptosis in OV cells, SKOV3 cells were treated with 0, 20, 40, or 60 μ M Icariside II for 48 h, and the levels of Fe²⁺, intracellular total iron concentration, and lipid ROS were evaluated. Our data showed that Icariside II treatment enhanced lipid ROS levels compared to those in the control group (Fig. 1A and B). Furthermore, Icariside II increased the Fe²⁺ levels (Fig. 1C) and intracellular total iron concentrations (Fig. 1D) in a dose-dependent manner. We also evaluated ferroptosis markers, including Ptgs2 and Chac1 using qRT-PCR. Icariside II significantly increased Ptgs2 and Chac1 expression in a dose-dependent manner in SKOV3 cells, as opposed to the 0 μ M Icariside II treatment group (Fig. 1E and F). Further mechanistic analysis revealed that Icariside II suppressed Cys, GSH, and GPX4 levels in a dose-dependent manner, compared to the 0 μ M treatment group (Fig. 1G-I), indicating that Icariside II induces ferroptosis in OV cells.

Multiple studies have revealed that SLC7A11 is a vital regulator of ferroptosis in several diseases, including OV [21]. Therefore, we investigated whether Icariside II regulates SLC7A11 expression in OV cells. As shown in Fig. 1J and K, Icariside II significantly inhibited SLC7A11 mRNA levels and protein expression in a dose-dependent manner in SKOV3 cells, suggesting that Icariside II induces ferroptosis in OV by regulating SLC7A11.

Upregulation of SLC7A11 reversed Icariside II-induced ferroptosis in OV cells

To further explore the roles of SLC7A11 in the ferroptosis of OV cells, control-plasmid, and SLC7A11-plasmid were transfected into SKOV3 cells. We observed that SLC7A11 was significantly upregulated in SLC7A11-plasmid transfected SKOV3 cells compared to the control-plasmid group (Fig. 2A and B). Considering the latent roles of Icariside II and SLC7A11 in OV cell ferroptosis,

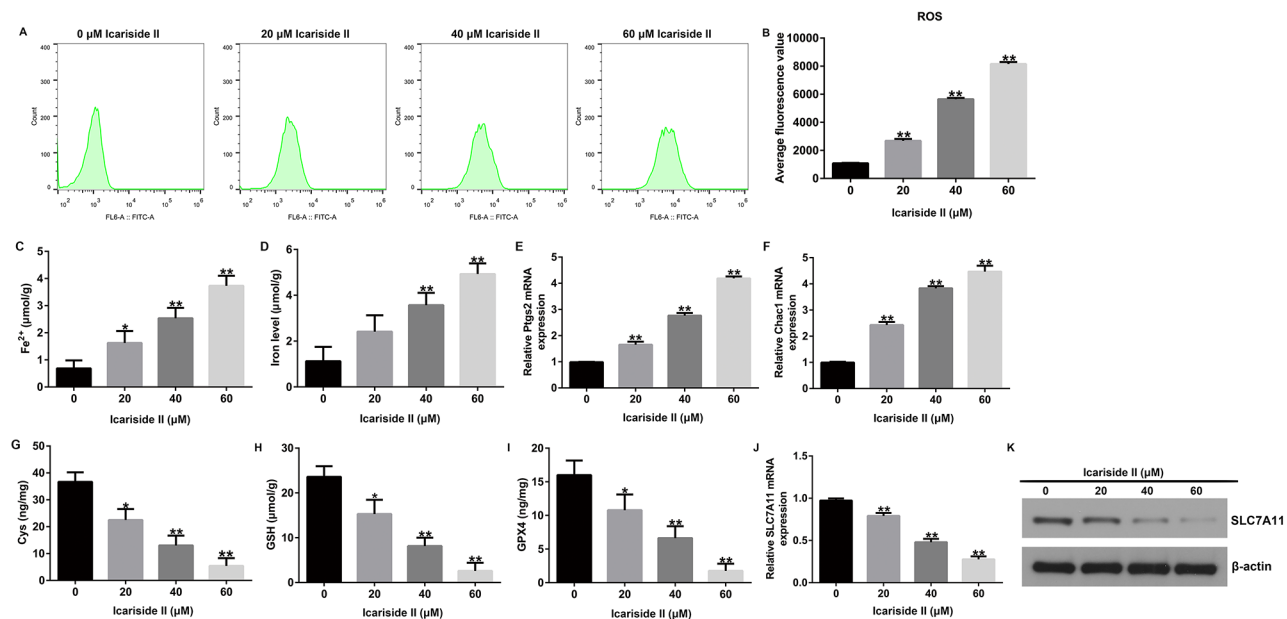


Fig. 1 Effects of Icariside II on SKOV3 cells ferroptosis. SKOV3 cells were exposed to various concentrations of Icariside II (0, 20, 40, 60 μM) for 48 h. (A and B) Statistical analysis of intracellular ROS content. Determination of ferrous (C) and total iron (D) levels in SKOV3 cells. (E and F) Levels of Pts2 and Chac1 were detected using qRT-PCR. Analysis of the levels of Cys (G), GSH (H), and GPX4 (I) in SKOV3 cells. (J and K) SLC7A11 levels were determined using RT-qPCR and Western blot analysis. * $P < 0.05$, ** $P < 0.01$ vs. Control. ROS, reactive oxygen species; Cys, cysteine; GSH, glutathione; GPX4, glutathione peroxidase 4

we evaluated whether Icariside II modulates the effect of SLC7A11 in OV cell ferroptosis. SKOV3 cells transfected with control-plasmid or SLC7A11-plasmid were treated with 60 μM Icariside II for 48 h. We found that Icariside II reduced SLC7A11 expression, and this inhibition was reversed in cells after SLC7A11-plasmid transfection (Fig. 2C and D). Our results suggest that SLC7A11 upregulation counteracts the effects of Icariside II on SLC7A11 expression.

Moreover, we investigated the effects of the SLC7A11-plasmid on Icariside II-induced ferroptosis in SKOV3 cells. Our results revealed that transfection with SLC7A11-plasmid reversed the effects of Icariside II on ferroptosis in OV cells, as evidenced by reduced lipid ROS levels, intracellular total iron concentration, and Fe²⁺ levels (Fig. 2E-G). Furthermore, the SLC7A11-plasmid decreased Pts2 and Chac1 expression (Fig. 2H-I) and increased Cys, GSH, and GPX4 levels in SKOV3 cells (Fig. 2J-L), compared to those in the control-plasmid group.

Icariside II inhibits the biological behavior of OV cells by inhibiting SLC7A11 expression

To illustrate the detailed mechanism of action of SLC7A11 and Icariside II in OV, the biological behaviors of SKOV3, including cell proliferation, apoptosis, migration, and invasion were assessed. Icariside II was found to decrease SKOV3 cell proliferation and promote apoptosis (Fig. 3A-C). Additionally, the expression

of apoptosis-related genes, including Bax and Bcl-2 was evaluated. The results demonstrated that Bax expression was upregulated and Bcl-2 expression was downregulated in Icariside II-treated SKOV3 cells (Fig. 3D-F). Furthermore, wound-healing and Transwell assays suggested that Icariside II inhibited SKOV3 cell migration and invasion (Fig. 3G and H). However, these effects were reversed in the SKOV3 cells treated with Icariside II and SLC7A11-plasmid. These results suggest that Icariside II exerts protective effects against OV by regulating SLC7A11 expression.

Icariside II inhibits OV tumor growth and induces ferroptosis by regulating SLC7A11 expression in vivo

Furthermore, an in vivo experiment was conducted to elucidate the regulatory roles of Icariside II and SLC7A11 in OV development. Xenograft tumor models were established (Fig. 4A). The xenograft tumor volumes and weights were calculated. The results suggested that Icariside II significantly inhibited tumor growth (Fig. 4B-C). Conversely, the Icariside II+SLC7A11-plasmid group exhibited increased tumor volumes and weights. Additionally, the effects of Icariside II and SLC7A11 on ferroptosis in vivo models were examined and we found that Icariside II markedly increased lipid ROS levels, intracellular Fe²⁺ concentrations, and total iron (Fig. 4D-F). Further analysis using qRT-PCR and biochemical detection assays indicated that Icariside II elevated Pts2 and Chac1 levels (Fig. 4G-H) and reduced Cys, GSH, and

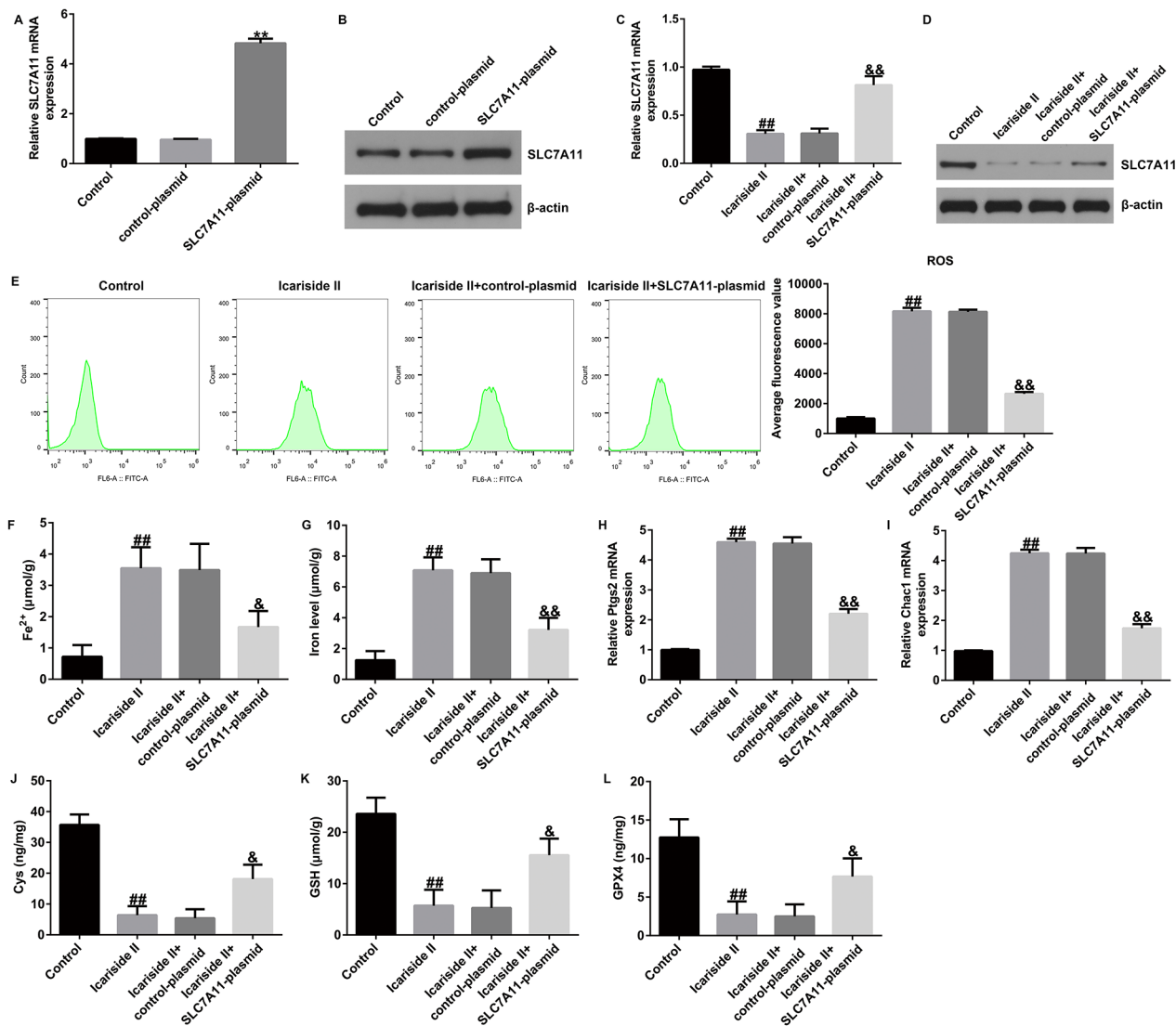


Fig. 2 Effects of SLC7A11-plasmid on Icariside II-induced ferroptosis in SKOV3 cells. **(A–B)** SLC7A11 levels in the control, control-plasmid, and SLC7A11-plasmid groups were assessed using RT-qPCR and Western blotting. **(C–D)** SLC7A11 levels in the control, Icariside II, Icariside II+control-plasmid, and Icariside II+SLC7A11-plasmid groups were analyzed using RT-qPCR and Western blotting. **(E)** Lipid ROS production in SKOV3 cells was evaluated using flow cytometry. Intracellular Fe^{2+} **(F)** and total iron **(G)** levels in SKOV3 cells were determined. **(H, I)** qRT-PCR analysis of Ptg2 and Chac1 levels. Cys **(J)**, GSH **(K)**, and GPX4 **(L)** levels in the SKOV3 cells. ** $P < 0.01$ vs. control-plasmid; ## $P < 0.01$ vs. Control; && $P < 0.05, 0.01$ vs. Icariside II+control-plasmid. ROS, reactive oxygen species; Cys, cysteine; GSH, glutathione; GPX4, glutathione peroxidase 4

GPX4 levels (Fig. 4I–K). However, these effects were reversed by SLC7A11-plasmid treatment. The expression of SLC7A11 in OV tissues was also evaluated. qRT-PCR and IHC results revealed that SLC7A11 overexpression reversed the effects of Icariside II on SLC7A11 expression, as confirmed by the enhanced SLC7A11 levels (Fig. 4L–M). These findings suggest that Icariside II inhibits tumor growth and induces ferroptosis in OV by down-regulating SLC7A11.

High SLC7A11 expression in patients with OV

Previous studies suggested that SLC7A11 plays a vital role in ferroptosis progression [22]. SLC7A11 expression in OV was explored using the TCGA database and IHC staining. We observed that SLC7A11 expression levels were significantly upregulated in most tumor tissues, compared to normal tissues, in the TCGA databases, including OV (Fig. 5A and B). Moreover, IHC analysis showed that SLC7A11 expression was elevated in OV tissues compared to adjacent non-tumor tissues (Fig. 5C). These observations further confirmed the regulatory roles of SLC7A11 in the OV progression and indicated

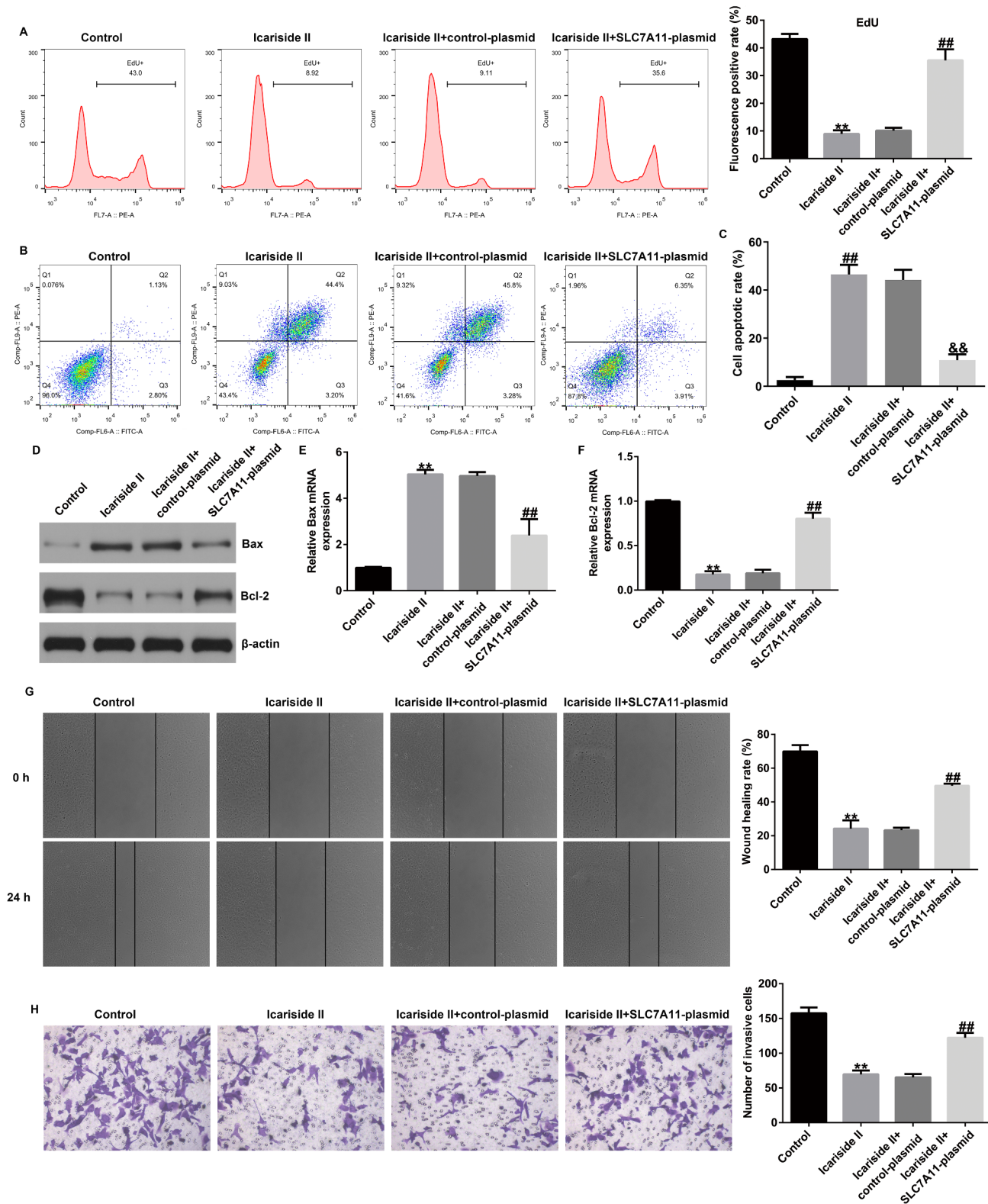


Fig. 3 Effects of SLC7A11-plasmid and Icariside II on SKOV3 cell proliferation, apoptosis, migration, and invasion. (A) SKOV3 cell proliferation was analyzed using the EdU assay. (B) Apoptosis was assessed by flow cytometry. (C) Quantification of apoptotic SKOV3 cells. (D) Western blot analysis of Bax and Bcl-2 expression. (E and F) Bax and Bcl-2 mRNA levels were analyzed using qRT-PCR. (G) Cell migration was evaluated using a wound-healing assay. (H) Transwell assays showing the invasive capacity of SKOV3 cells. $**P < 0.01$ vs. Control; $###P < 0.01$ vs. Icariside II + control-plasmid

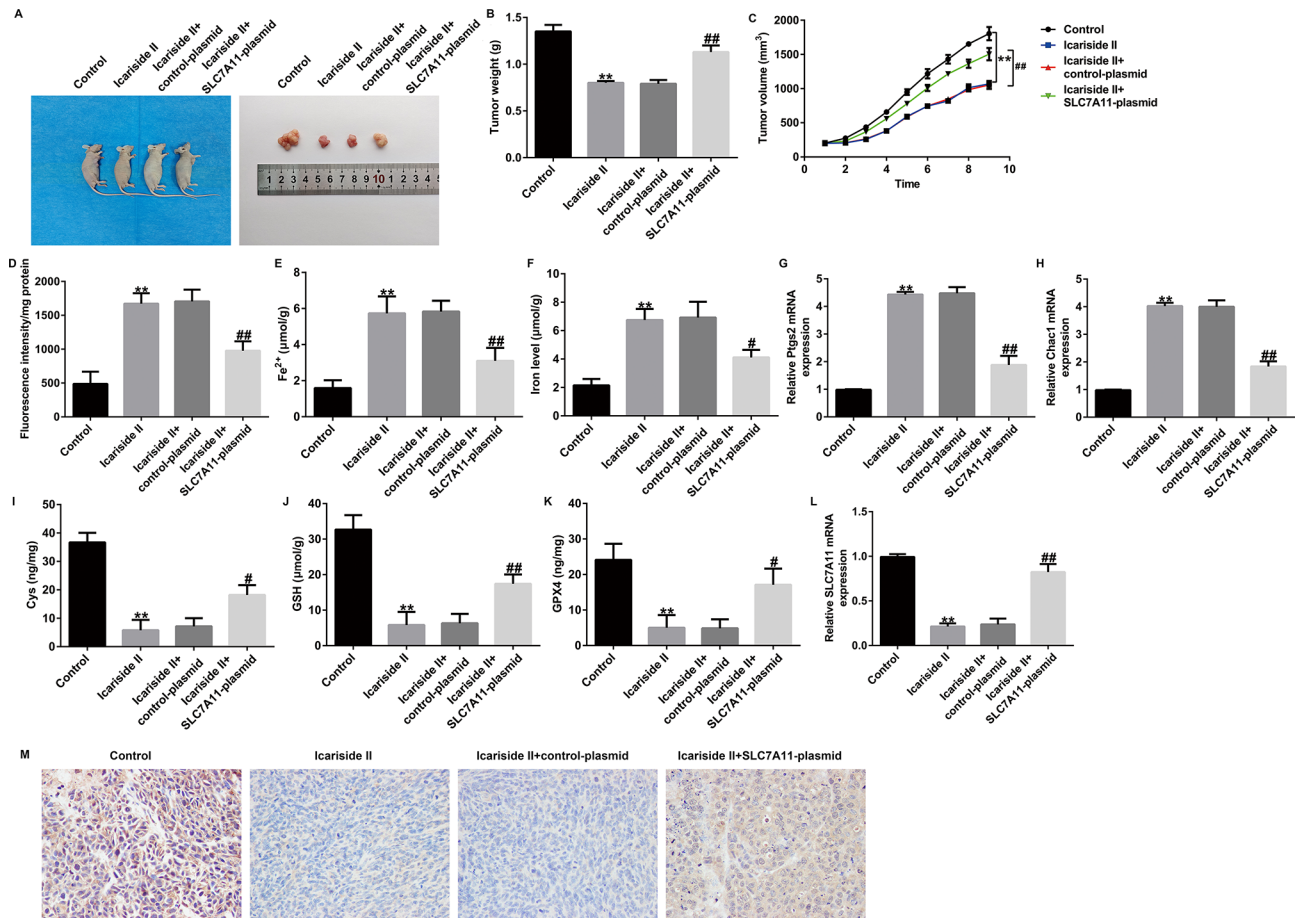


Fig. 4 Effects of SLC7A11-plasmid and Icariside II on tumor growth and ferroptosis in vivo. **(A)** Representative images of tumors. **(B, C)** Tumor volumes and weights were recorded. **(D)** Lipid ROS production in tumor tissues was assessed. **(E)** Ferrous and **(F)** total iron levels in SKOV3 cells. **(G, H)** The mRNA levels of PtgS2 and Chac1 in SKOV3 cells were analyzed using qRT-PCR. Detection of the levels of Cys **(I)**, GSH **(J)**, and GPX4 **(K)** levels in SKOV3 cells. **(L)** qRT-PCR analysis of SLC7A11 expression. **(M)** Immunohistochemical images obtained after staining with SLC7A11. ****** $P < 0.01$ vs. Control; #, **##** $P < 0.05, 0.01$ vs. Icariside II+control-plasmid. ROS, reactive oxygen species; Cys, cysteine; GSH, glutathione; GPX4, glutathione peroxidase 4

that Icariside II may be a promising therapeutic agent for treating OV.

Discussion

OV is one of the three most common gynecological malignancies, and its pathogenesis involves multiple molecules, including genes, miRNAs, and lncRNAs [23, 24]. Surgery, chemotherapy, and radiotherapy are the primary treatment approaches for OV [25, 26]. Unfortunately, the prognosis remains poor, because of the advanced stage at diagnosis and the limited treatment options available. Yu et al. reported that FMO2 could serve as a predictive biomarker for OV [27]. Scaletta et al. suggested the role of the novel biomarker, HE4, in the diagnosis and prognosis of OV [28]. These findings emphasize the need to identify novel treatment strategies for OV.

Herba Epimedii is a traditional Chinese medicine with a long history and icariin is one of its main active ingredients. Icariin has been reported to play vital roles in knee osteoarthritis, cardiovascular and neurological diseases,

and gastric cancer [15]. An increasing number of studies suggest that Icariside II, the main metabolite of icariin, has anti-inflammatory and antioxidant activities. Jiang et al. reported the therapeutic effects of icariin and Icariside II on diabetes mellitus and its complications [29]. Moreover, Zhang et al. suggested that icariin and Icariside II reciprocally stimulate osteogenesis and inhibit adipogenesis in multipotent stromal cells through ERK signaling [30]. In recent years, studies have shown that Icariside II plays an anti-cancer role in a variety of tumors [18, 19, 31, 32]. Icariside II has been reported to inhibit resistance to cisplatin in ovarian cancer cells by suppressing autophagy via downregulating HIF-1 α /ATG5 axis [33]. However, the role and underlying molecular mechanism of Icariside II in OV remains largely unclear. Recent studies have found a close relationship between miR-144-3p and SLC7A11, showing that miR-144-3p regulates SLC7A11 expression [34]. Based on these findings, we hypothesized that Icariside II may regulate SLC7A11 expression in OV. Ferroptosis is mainly caused by lethal lipid peroxidation due to

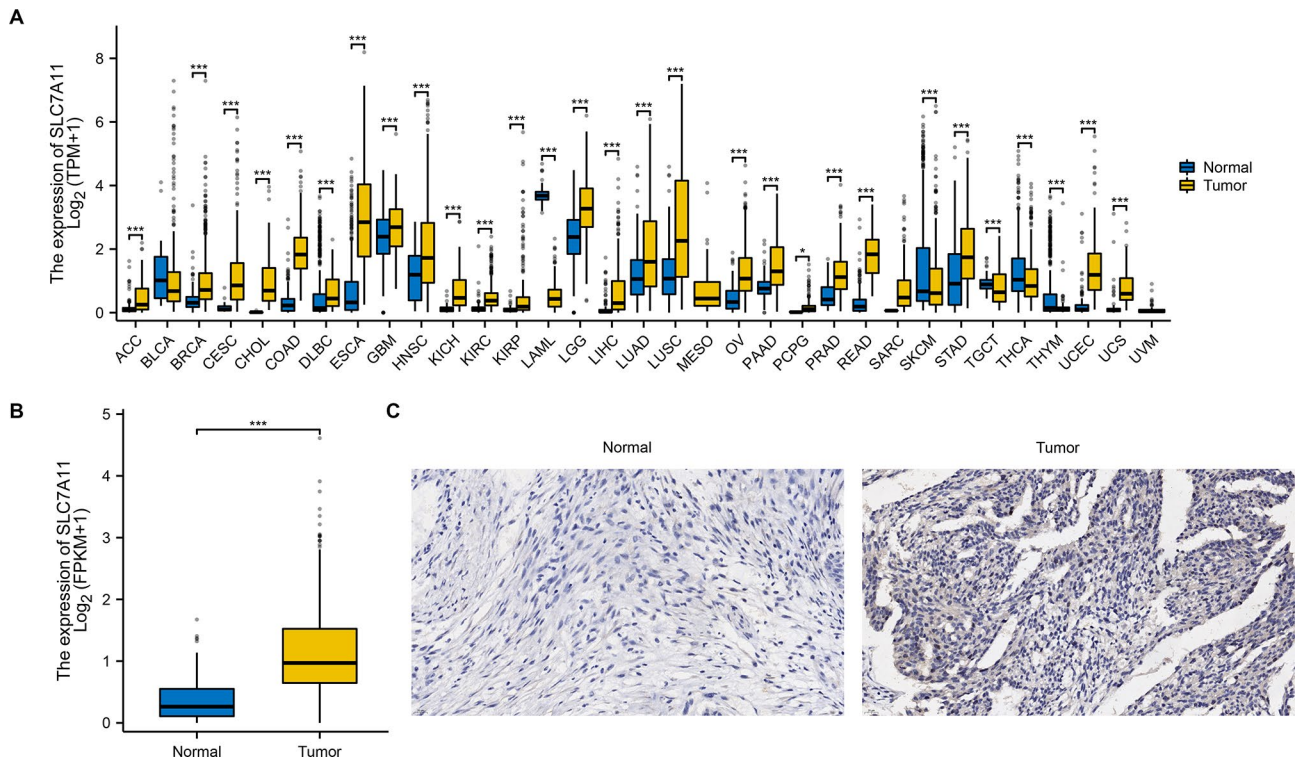


Fig. 5 Expression of SLC7A11 in ovarian cancer patients. **(A)** Pan-cancer SLC7A11 expression status. **(B)** SLC7A11 expression in ovarian cancer tissues compared with that in normal tissues. **(C)** Immunohistochemical images of SLC7A11 expression in ovarian cancer tissues and adjacent normal tissues from patients with ovarian cancer. *** $P < 0.001$

an imbalance in redox homeostasis, and ROS production plays a vital role in ferroptosis. The cystine/glutamic acid reverse transport system, Xc⁻, composed of SLC7A11 and SLC3A2 subunits, is closely linked to ferroptosis. Yang et al. revealed that STAT6 inhibits ferroptosis and alleviates acute lung injury by regulating the P53/SLC7A11 pathway [35]. Moreover, Koppula et al. suggested a relationship between the cystine transporter SLC7A11/xCT, ferroptosis, and cancer therapy [36]. This study was designed to explore whether Icariside II induces ferroptosis in OV cells by regulating SLC7A11 expression.

In this study, SKOV3 cells were treated with Icariside II (0, 20, 40, or 60 μ M) for 48 h, and ferroptosis-related markers were analyzed. Consistent with previous research, we observed that Icariside II elevated the levels of Fe²⁺ lipid ROS, and intracellular total iron concentrations in a dose-dependent manner. Moreover, Ptg2 and Chac1 expressions were upregulated in Icariside II-treated SKOV3 cells compared to the control group. GSH and GPX4 are established regulators of ferroptosis. Yang et al. revealed the involvement of the GSH-GPX4 pathway in ferroptosis of the retinal pigment epithelium [37]. Furthermore, Yang et al. have suggested that Maresin1 protects against ferroptosis-induced liver injury through ROS inhibition and Nrf2/HO-1/GPX4 activation [38]. To further assess the regulatory factors involved in

ferroptosis, we measured the levels of Cys, GSH, and GPX4, in SKOV3 cells. Our findings suggest that Icariside II significantly reduced Cys, GSH, and GPX4 levels compared to the control group.

Multiple studies have suggested that SLC7A11 plays an important role in ferroptosis in many diseases, including OV [39, 40]. Therefore, we investigated whether Icariside II regulated SLC7A11 expression in OV cells. We observed that Icariside II inhibited SLC7A11 mRNA levels and expression in a dose-dependent manner in SKOV3 cells. This inhibition was reversed after SLC7A11-plasmid transfection. Further findings suggested that the upregulation of SLC7A11 reversed the effects of Icariside II on ferroptosis in OV cells. To further illustrate the detailed mechanism of action of SLC7A11 and Icariside II in OV, we assessed the biological behavior of SKOV3 cells, including cell proliferation, apoptosis, migration, and invasion. We found that Icariside II exposure resulted in a dose-dependent decrease in the viability, migration, and invasion of SKOV3 cells. A marked dose-dependent increase in apoptosis was observed in the Icariside II-treated SKOV3 cells. Proteins in the Bcl-2 family exhibit either pro-apoptotic or anti-apoptotic activities, with the Bcl-2/Bax ratio serving as a marker of apoptosis [41]. Our results demonstrated that Bax and Bcl-2 were upregulated in Icariside II-treated

SKOV3 cells. However, these findings were reversed in the Icariside II + SLC7A11-plasmid-treated SKOV3 cells. Collectively, our findings revealed that Icariside II has the potential to inhibit OV cell growth and metastasis by regulating SLC7A11 expression.

Furthermore, Icariside II substantially suppressed the volume and weight of OV xenografts *in vivo*. Sun et al. reported that Icariside II suppresses cervical cancer cell migration through JNK-modulated matrix metalloproteinase-2/9 inhibition *in vitro* and *in vivo* [42]. These findings, together with our results, suggested that Icariside II suppresses tumor formation in OV *in vivo*. Additionally, we provide strong evidence to support the role of Icariside II in SLC7A11-regulated OV ferroptosis *in vivo*. As confirmed by the increased intracellular concentrations of Fe²⁺, total iron, and lipid ROS levels, and elevated Ptgs2 and Chac1 levels, as well as reduced Cys, GSH, and GPX4 levels in Icariside II-treated SKOV3 cells, we observed the opposite results in the SLC7A11-plasmid group. Further, qRT-PCR and IHC assays revealed that overexpression of SLC7A11 reversed the effects of Icariside II on SLC7A11 expression, suggesting that Icariside II inhibits tumor growth and induces ferroptosis in OV by downregulating SLC7A11. SLC7A11 is a cystine/glutamate exchanger involved in the synthesis of the cellular antioxidant, glutathione. To further analyze the roles of SLC7A11 in OV tumorigenesis, we evaluated SLC7A11 expression in OV tissues and adjacent non-tumor tissues by IHC and found that SLC7A11 expression was upregulated in OV tissues, compared to normal tissues. Data from TCGA databases further confirmed that SLC7A11 expression levels were elevated in most tumor tissues compared with normal tissues, including OV. Higher SLC7A11 expression was observed in tumor samples, which was correlated with the pathological parameters of patients with OV. We will further explore the combination and mode of action of SLC7A11 and Icariside II, as well as their downstream cascade feedback patterns in OV in our next research.

In summary, we demonstrated that Icariside II induces ferroptosis in SKOV3 cells and plays a vital tumor-suppressive role in ovarian carcinogenesis, primarily by regulating SLC7A11. Our study provides critical insights into the use of Icariside II in the treatment of OV.

Abbreviations

Cys	Cysteine
GSH	Glutathione
GPX4	Glutathione peroxidase 4
IHC	Immunohistochemistry
OS	Overall survival
OV	Ovarian cancer
RIPA	Radioimmunoprecipitation assay
ROS	Reactive oxygen species
SD	Standard deviation
TCGA	The Cancer Genome Atlas

Supplementary Information

The online version contains supplementary material available at <https://doi.org/10.1186/s13048-025-01650-1>.

Supplementary Material 1

Supplementary Material 2

Acknowledgements

Not applicable.

Author contributions

Donglan Yuan and Ting Guo: Conceptualization, Formal analysis, Project administration, Writing-original draft, and Writing-review & editing. Xiaotong Zhu, Weiwei Song, and Dengyun Nie: Investigation, Methodology, Software, and Writing-review & editing. Hong Yu: Supervision, Visualization and Writing-review & editing. All authors have read and approved the final manuscript.

Funding

This study was supported by the Taizhou Science and Technology Support Plan social development project (grant no. TS202003), the 2024 Annual Taizhou City Sixth Phase "311 Project" Training Object Research Funding Program, and the 2024 Annual Research Project of Taizhou Clinical Medical College, Nanjing Medical University (grant no. TZKY20240206).

Data availability

No datasets were generated or analysed during the current study.

Declarations

Human ethics and consent to participate declarations

This study was approved by the Ethics Committee of the Affiliated Taizhou People's Hospital of Nanjing University of Traditional Chinese Medicine in accordance with the Declaration of Helsinki. Written informed consent was obtained from the patient before surgery.

Competing interests

The authors declare no competing interests.

Received: 24 July 2024 / Accepted: 16 March 2025

Published online: 05 April 2025

References

1. Elayapillai S, Ramraj S, Benbrook DM, et al. Potential and mechanism of Mebendazole for treatment and maintenance of ovarian cancer. *Gynecol Oncol*. 2021;160:302–11.
2. Bray F, Laversanne M, Sung H, et al. Global cancer statistics 2022: GLOBOCAN estimates of incidence and mortality worldwide for 36 cancers in 185 countries. *CA Cancer J Clin*. 2024;74:229–63.
3. Santos ML, Pais AS, Almeida ST. Fertility preservation in ovarian cancer patients. *Gynecol Endocrinol*. 2021;37:483–9.
4. Monavarian M, Elhaw AT, Tang PW, et al. Emerging perspectives on growth factor metabolic relationships in the ovarian cancer Ascites environment. *Semin Cancer Biol*. 2022;86:709–19.
5. Porter R, Matulonis UA. Immunotherapy for ovarian cancer. *Clin Adv Hematol Oncol*. 2022;20:240–53.
6. Li H, Liu Y, Wang Y, Zhao X, Qi X. Hormone therapy for ovarian cancer: emphasis on mechanisms and applications (Review). *Oncol Rep*. 2021;46.
7. Lee JY, Kim BG, Kim JW, et al. Biomarker-guided targeted therapy in platinum-resistant ovarian cancer (AMBITION; KGOG 3045): a multicentre, open-label, five-arm, uncontrolled, umbrella trial. *J Gynecol Oncol*. 2022;33:e45.
8. Gao W, Wang X, Zhou Y, Wang X, Yu Y. Autophagy, ferroptosis, pyroptosis, and necroptosis in tumor immunotherapy. *Signal Transduct Target Ther*. 2022;7:196.
9. Zhou B, Liu J, Kang R, Klionsky DJ, Kroemer G, Tang D. Ferroptosis is a type of autophagy-dependent cell death. *Semin Cancer Biol*. 2020;66:89–100.

10. Bai T, Li M, Liu Y, Qiao Z, Wang Z. Inhibition of ferroptosis alleviates atherosclerosis through attenuating lipid peroxidation and endothelial dysfunction in mouse aortic endothelial cell. *Free Radic Biol Med*. 2020;160:92–102.
11. Zhao L, Zhou X, Xie F, et al. Ferroptosis in cancer and cancer immunotherapy. *Cancer Commun (Lond)*. 2022;42:88–116.
12. Fang X, Ardehali H, Min J, Wang F. The molecular and metabolic landscape of iron and ferroptosis in cardiovascular disease. *Nat Rev Cardiol*. 2023;20:7–23.
13. Qi W, Li Z, Xia L, et al. LncRNA GABPB1-AS1 and GABPB1 regulate oxidative stress during erastin-induced ferroptosis in HepG2 hepatovellular carcinoma cells. *Sci Rep*. 2019;9:16185.
14. He L, Liu YY, Wang K, et al. Tanshinone IIA protects human coronary artery endothelial cells from ferroptosis by activating the NRF2 pathway. *Biochem Biophys Res Commun*. 2021;575:1–7.
15. Dong C, Shi J, Chen X, et al. Beneficial effects of herba epimedii on ovariectomized rats by down-regulating PGE2 and ADRbeta-2R expression. *Minerva Med*. 2019;110:595–7.
16. Bi Z, Zhang W, Yan X. Anti-inflammatory and immunoregulatory effects of Icaria and Icaritin. *Biomed Pharmacother*. 2022;151:113180.
17. Song J, Feng L, Zhong R, et al. Icariside II inhibits the EMT of NSCLC cells in inflammatory microenvironment via down-regulation of Akt/NF-kappaB signaling pathway. *Mol Carcinog*. 2017;56:36–48.
18. Yuan D, Guo T, Qian H, et al. Icariside II suppresses the tumorigenesis and development of ovarian cancer by regulating miR-144-3p/IGF2R axis. *Drug Dev Res*. 2022;83:1383–93.
19. Yu R, Zhou Y, Shi S, Wang X, Huang S, Ren Y. Icariside II induces ferroptosis in renal cell carcinoma cells by regulating the miR-324-3p/GPX4 axis. *Phyto-medicine*. 2022;102:154182.
20. Yuan Y, Yucai L, Lu L, Hui L, Yong P, Haiyang Y. Acrylamide induces ferroptosis in HSC-T6 cells by causing antioxidant imbalance of the XCT-GSH-GPX4 signaling and mitochondrial dysfunction. *Toxicol Lett*. 2022;368:24–32.
21. Zhang X, Zheng X, Ying X, Xie W, Yin Y, Wang X. CEBPG suppresses ferroptosis through transcriptional control of SLC7A11 in ovarian cancer. *J Transl Med*. 2023;21:334.
22. Hong T, Lei G, Chen X, et al. PARP Inhibition promotes ferroptosis via repressing SLC7A11 and synergizes with ferroptosis inducers in BRCA-proficient ovarian cancer. *Redox Biol*. 2021;42:101928.
23. Wang Y, Shao F, Chen L. miR-425 regulates ovarian cancer proliferation, metastasis, and apoptosis by repressing PAK4 expression. *Asia Pac J Clin Oncol*. 2022;18:76–83.
24. Tao F, Tian X, Lu M, Zhang Z. A novel lncRNA, lnc-OV1, promotes ovarian cancer cell proliferation and migration by sponging miR-34a and miR-34c. *J Genet Genomics*. 2018;45:137–45.
25. Wang J, Zhang R, Zhang B, et al. MiR-135b improves proliferation and regulates chemotherapy resistance in ovarian cancer. *J Mol Histol*. 2022;53:699–712.
26. Johns EA, Stanley JA, Toboni MD, et al. Radiation therapy for vaginal and perirectal lesions in recurrent ovarian cancer. *Gynecol Oncol Rep*. 2021;37:100808.
27. Yu S, Yang R, Xu T, Li X, Wu S, Zhang J. Cancer-associated fibroblasts-derived FMO2 as a biomarker of macrophage infiltration and prognosis in epithelial ovarian cancer. *Gynecol Oncol*. 2022.
28. Wang ZX, Ding SN. Duplex-immunoassay of ovarian cancer biomarker CA125 and HE4 based carbon Dot decorated dendritic mesoporous silica nanoparticles. *Analyst*. 2023;148:683–9.
29. Jiang W, Ding K, Yue R, Lei M. Therapeutic effects of Icaria and Icariside II on diabetes mellitus and its complications. *Crit Rev Food Sci Nutr*. 2023:1–26.
30. Zhang D, Zhao N, Wan C, Du J, Lin J, Wang H. Icaria and Icariside II reciprocally stimulate osteogenesis and inhibit adipogenesis of multipotential stromal cells through ERK signaling. *Evid Based Complement Alternat Med*. 2021;2021:8069930.
31. He K, Wang J, Zhou Y, Huang Z, Xie N, Li Y, Hu H, Chen Z, He Y, Tang Y. Network Pharmacology analysis of Icariside II against bladder cancer. *Eur J Pharmacol*. 2023;955:175914.
32. Xu F, Wu Q, Li L, Gong J, Huo R, Cui W. Icariside II: anticancer potential and molecular targets in solid cancers. *Front Pharmacol*. 2021;12:663776.
33. Zhou Y, Liu T, Wu Q, Wang H, Sun Y. Baohuoside I inhibits resistance to cisplatin in ovarian cancer cells by suppressing autophagy via downregulating HIF-1alpha/ATG5 axis. *Mol Carcinog*. 2023;62:1474–86.
34. Li Y, Han L, Hou B, Ji Y. Novel ginsenoside monomer RT4 promotes colitis repair in mice by regulating miR-144-3p/SLC7A11 signaling pathway. *Fundam Clin Pharmacol*. 2023.
35. Yang Y, Ma Y, Li Q, et al. STAT6 inhibits ferroptosis and alleviates acute lung injury via regulating P53/SLC7A11 pathway. *Cell Death Dis*. 2022;13:530.
36. Koppula P, Zhuang L, Gan B. Cystine transporter SLC7A11/xCT in cancer: ferroptosis, nutrient dependency, and cancer therapy. *Protein Cell*. 2021;12:599–620.
37. Yang M, Tsui MG, Tsang J, et al. Involvement of FSP1-CoQ(10)-NADH and GSH-GPx-4 pathways in retinal pigment epithelium ferroptosis. *Cell Death Dis*. 2022;13:468.
38. Yang W, Wang Y, Zhang C, et al. Maresin1 protect against Ferroptosis-Induced liver injury through ROS Inhibition and Nrf2/HO-1/GPX4 activation. *Front Pharmacol*. 2022;13:865689.
39. Qin K, Zhang F, Wang H, et al. CircRNA circSnx12 confers cisplatin chemoresistance to ovarian cancer by inhibiting ferroptosis through a miR-194-5p/SLC7A11 axis. *BMB Rep*. 2023;56:184–9.
40. Fantone S, Piani F, Olivieri F, Rippo MR, Sirico A, Di Simone N, Marziani D, Tossetta G. Role of SLC7A11/xCT in ovarian cancer. *Int J Mol Sci*. 2024;25(1):587.
41. Warren C, Wong-Brown MW, Bowden NA. BCL-2 family isoforms in apoptosis and cancer. *Cell Death Dis*. 2019;10:177.
42. Sun YS, Thakur K, Hu F, Cespedes-Acuna CL, Zhang JG, Wei ZJ. Icariside II suppresses cervical cancer cell migration through JNK modulated matrix metalloproteinase-2/9 Inhibition in vitro and in vivo. *Biomed Pharmacother*. 2020;125:110013.

Publisher's note

Springer Nature remains neutral with regard to jurisdictional claims in published maps and institutional affiliations.